SOFC Modeling Considering Internal Reforming by a Global Kinetics Approach

Andersson, Martin; Yuan, Jinliang; Sundén, Bengt

Published in:
Solid Oxide Fuel Cells, Eleventh International Symposium (SOFC XI)

2009

SOFC Modeling Considering Internal Reforming by a Global Kinetics Approach

M. Andersson [a], J. Yuan [a], B. Sundén [a]

[a] Department of Energy Sciences, Lund University, SE-221 00 Lund, Sweden

Fuel cells (FCs) are promising for future energy systems, since they are energy efficient and fuel can be produced locally. When hydrogen is used as fuel, there are no emissions of greenhouse gases. In this study a two dimensional CFD (COMSOL Multiphysics) is employed to study the effect from porous material surface area ratio on reforming reaction rates and gas species distributions for an anode-supported solid oxide fuel cell (SOFC). FCs can be considered as multifunctional energy devises, combining (electro-) chemical reactions, heat exchange, gas- and ionic transport. All these functions are strongly integrated, making modeling an important tool to understand the couplings between mass-, heat-, momentum transport and chemical reactions. Steam reforming takes place at the nickel material surfaces in the anode and water-gas shift reaction occurs where fuel gas is present. Benefit from the internal reforming is that the energy conversion efficiency will be higher, compared to the case of pure hydrogen as fuel.

Introduction and Problem Statement

Fuel cells (FCs) produce electricity and heat directly from chemical conversion of fuel and oxidant energies by electrochemical reactions (1-2). The fuel cell is not a new invention, because the electrochemical process was discovered already in 1839. However the first real fuel cell system was not designed and built until the 1950s. The interest in fuel cells have been growing exponentially, concerning amount of scientific papers, after year 2000 (3). Among the various types of FCs, the solid oxide fuel cell (SOFC) has attained significant interest due to its high efficiency and low emissions of pollutants to the environment. High temperature operation offers many advantages, such as high electrochemical reaction rate, flexibility of using various fuels and tolerance to impurities. SOFC has in general either planar or tubular configurations (1-2, 4), and its performance depends on thermal, electro-chemical, mechanical and chemical phenomena (5).

In an electrode-supported SOFC either the anode or cathode is relatively thick and works as support material. This design makes it possible to have a very thin electrolyte, i.e. the ohmic losses decreases and the temperature can be lowered to 600-800 °C. Fuel cells working in this temperature range are classified as intermediate temperature (IT) (1-2) if compared to conventional SOFCs that operate between 800 and 1000 °C (6).

SOFCs can work with a variety of fuels, e.g., hydrogen, carbon monoxide, methane and combinations of these (7). Oxygen is reduced in the cathode, eqn. [1]. The oxygen ions are transported through the electrolyte, but the electrons are prevented to pass

through the electrolyte. The electrochemical reactions, eqns. [2]-[3], take place in the anodic three-phase boundary (TPB). Methane needs to be reformed, eqn. [4], before the electrochemical reactions (8). Carbon monoxide can be oxidized in the electrochemical reaction, eqn. [3], but can also react with water (eqn. [5]). The reactions described here are the overall reactions, more detailed reaction mechanisms can be found in (8-9). Note that methane is not participating in the electrochemical reactions at the anodic TPB, it is catalytically converted, within the anode, into carbon monoxide and hydrogen, which are used as fuel in the electrochemical reactions (10).

$$O_2 + 4e^- \Leftrightarrow 2O^{2-} \quad [1]$$

$$H_2 + O^{2-} \Leftrightarrow H_2O + 2e^- \quad [2]$$

$$CO + O^{2-} \Leftrightarrow CO_2 + 2e^- \quad [3]$$

$$CH_4 + H_2O \Leftrightarrow 3H_2 + CO \quad [4]$$

$$CO + H_2O \Leftrightarrow H_2 + CO_2 \quad [5]$$

Due to complex processes involved in fuel cells, it is not possible to solve the equations describing the physical phenomena analytically, a numerical approach, e.g. the Finite Element Method, needs to be applied to solve the equations in an approximate way (11). A model that describes physical (mass-, heat- and momentum) phenomena inside an anode-supported SOFC is developed, to deeply understand the effect of design and operating parameters. A two-dimensional numerical calculation procedure (CFD approach) is further applied. This study focuses on the effect of active surface area ratio on the steam reforming reaction. Temperature dependent thermal-physical properties are taken into account as well. The temperature distribution in the solid phase and gas phase are calculated separately, based on the LTNE approach.

Mathematical Model

A two-dimensional model for an anode-supported SOFC is developed and implemented in the commercial software, COMSOL Multiphysics (version 3.5). Equations for momentum-, mass- and heat transport are solved simultaneously. The geometry is defined in Table I and a sketch of the modeled cell can be seen in Fig 1. Note the difference in scale between the cell length (x-direction, as in Fig. 1) and various component thicknesses (y- direction, as in Fig. 1). It should be mentioned that the model in this study is 2D only, and the connection between the electrodes and interconnect can not be explicitly observed in this case.

Two approaches for defining the electrochemical reactions can be found in the literature, either as source terms in the governing equations (12-13) or as interface conditions defined at the electrode/electrolyte interfaces (14-15). The electrochemical reactions are simplified in this work and defined as interface conditions, and this approach affects the momentum-, heat transfer- and mass transport equations. This approach can be used, because the thickness of the active layer is sufficiently thin, compared to the thickness of the electrode (14-15).

TABLE I. Cell geometry

Cell Component	Thickness
Cell length	0.1 m
Fuel channel height	1 mm
Air channel height	1 mm
Anode thickness	500 μm
Cathode thickness	50 μm
Electrolyte thickness	20 μm
Interconnect thickness	500 μm

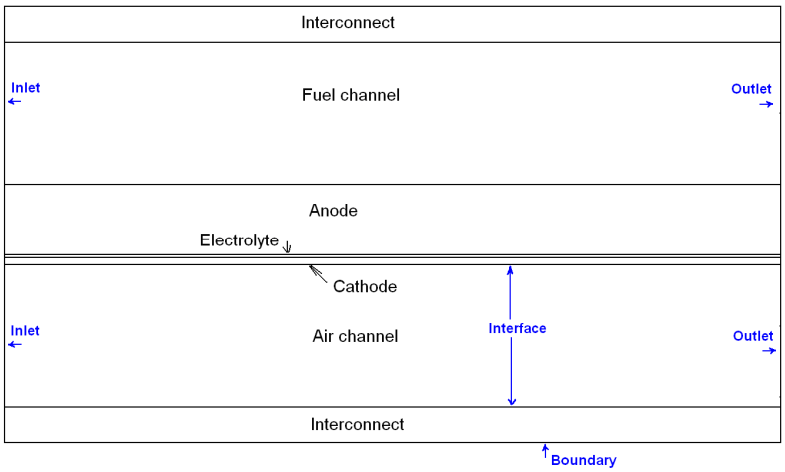

Figure 1. Sketch of an anode-supported SOFC, not to scale.

Momentum transport

The gases flow inside the fuel cell components, such as in the air and fuel channels, and the porous electrodes. A traditional modeling approach for such a system consists of solving the Darcy's equation in the porous medium and the Navier-Stokes equations in the channels separately. The problem with such an approach is to define interface conditions at the interface between the two domains. It is hard to define this tangential velocity component. To avoid this problem the Darcy-Brinkman equation is introduced and solved for the gas flow in the fuel and air channels, and in the porous materials simultaneously (16,17). The Darcy-Brinkman equation (eq.[6]) is transformed into the standard Navier-Stokes equation when ($\kappa \to \infty$) and ($\varepsilon_p = 1$), and into the Darcy equation as ($Da \to 0$). *Da* is the Darcy number. The derivation of Navier-Stokes equation and Darcy equation from Darcy-Brinkman equation can be found in (16).

$$\left(\frac{\mu}{\kappa} + \rho \cdot \nabla \mathrm{u}\right)\mathrm{u} - \nabla\left[-p + \frac{1}{\varepsilon_p}\left\{\mathbf{T} - \left(\lambda - \kappa_{dv}\right)\left(\nabla \mathrm{u}\right)\right\}\right] = \mathbf{F} \qquad [6]$$

where $\mathbf{F}$ is the volume force vector, κ is the permeability of the porous medium, ε_p the porosity, μ the dynamic viscosity, u the velocity vector and $\mathbf{T}$ the viscous stress tensor $\left(\mathbf{T} = v\left(\nabla \mathrm{u} + \left(\nabla \mathrm{u}\right)^T\right)\right)$. κ_{dv} (deviation from thermodynamic equilibrium) is by default set to zero, which means that the fluid particles are in equilibrium with their surrounding. λ is the second viscosity and is, for gases, normally assumed as: $\lambda = -2/3\ \mu$ (18). The densities and viscosities for the participating gases are dependent on local concentration and

temperature, and calculated as described in (19-20). The gas inlet velocities are defined as a laminar flow profile for an oxygen surplus factor of 4 and a fuel consumption of 80 % (mole). The outlet are defined as pressure (= 1 atm). A gas velocity effect is calculated to encounter for the electrochemical reactions at the electrolyte/electrode interfaces (19,20).

Mass transport

The Maxwell-Stefan equation for mass diffusion and convection is used to describe the mass transport phenomena for the gases inside the fuel cell (17). The Maxwell-Stefan equation is a simplified equation compared to "Dusty Gas Model", since the Knudsen diffusion (collisions between gas molecules and the porous material) is neglected. The reason for this treatment is to reduce the calculation cost, and this model is already predefined in the commercial software COMSOL Multiphysics, as used in this work. The Maxwell-Stefan equation is solved for the fuel and air channels and the electrodes.

$$\nabla\left(-\rho \cdot w_i \sum^{n} \overline{D}_{ij} \cdot \nabla x_j \left(x_j - w_j\right)\frac{\nabla p}{p} \cdot \mathrm{u} - D_i^T \cdot \frac{\nabla T}{T}\right) + \rho \cdot \mathrm{u} \cdot \nabla w_j = S_i \qquad [7]$$

where w is the mass fraction, x the mole fraction, n the number of species, D_i^T the thermal diffusion coefficient and D_{ij} the Maxwell-Stefan binary diffusion coefficient. S_i, source term by chemical reaction, is only defined for the internal reforming reactions, because the electrochemical reactions are assumed to take place, at the interfaces between the electrolyte and electrodes. The electrochemical reactions occur in reality at an active reaction surface area, the TPB, where gas, ionic and electronic phases meet. The diffusion coefficient is dependent on temperature and is calculated as described in (19-20). On the air side nitrogen and oxygen are involved and only one Maxwell-Stefan diffusion coefficient needs to be calculated. On the fuel side methane, water, hydrogen, carbon monoxide and carbon dioxide are present and 10 pairs of Maxwell-Stefan diffusion coefficient needs to be calculated. The boundary conditions for the mass transport equation are defined as mass fraction for the gas channel inlets, the outlets are defined as convective flux (19-20).

Heat transport

The temperature distribution is calculated separately for the gas phase (in air and fuel channels and electrodes) and for the solid phase (interconnect, electrodes and electrolyte). Heat is transferred between the phases at the channel walls and in the porous electrodes. The general heat conduction equation is used to calculate the temperature distribution for the solid materials, i.e., electrolyte, interconnect and electrodes (17):

$$\nabla\left(-k_s \cdot \nabla T_s\right) = Q_s \qquad [8]$$

where k_s is the thermal conductivity of the solids, T_s the solid temperature and Q_s the heat source (heat transfer between the solid and gas phases, and heat generation due to ohmic polarization). Note that heat generated due to ohmic polarization is assumed to enter the solid phase (as a part of Q_s), heat generation due to electrochemical reactions, concentration and activation polarization are simplified and defined as the interface

conditions, such as for the mass transport. The temperature distribution for the gas mixtures in the fuel and air channels and in the porous electrodes is calculated as (17):

$$\nabla\left(-k_g \cdot \nabla T_g\right) = Q_g - \rho_g \cdot c_{p,g} \cdot \mathrm{u} \cdot \nabla T_g \qquad [9]$$

where $c_{p,g}$ is the gas phase heat capacity, T_g the temperature in the gas phase and Q_g the heat transfer between the gas and solid phases. Because the Reynolds number is very low, the heat transfer coefficient ($h_{s,g,por}$) in the porous electrodes (spherical particles are assumed) can be calculated as (21):

$$h_{s,g,por} = \frac{2 \cdot k_g}{d_p} \qquad [10]$$

where d_p is the electrode particle diameter and k_g the gas conductivity. The heat transfer between the gas phase and solid phase depends on the temperature difference and the particle surface area as (22):

$$Q_g = h_v \cdot \left(T_g - T_s\right) = SA \cdot h_{s,g,por} \cdot \left(T_g - T_s\right) \qquad [11]$$

where h_v is the volume heat transfer coefficient and SA the surface area (760 000 m^2/m^3 for the cathode and 619 000 m^2/m^3 for the anode (23)). Note that it is not the same surface area that is used for heat transfer between the solid- and gas phase and for catalytic steam reforming reaction. In reality the surface area for heat transfer is expected to be higher (because not all the surface is covered with active Ni catalyst), this difference can be neglected since the maximum temperature difference between the phases is less than 1 K. The heat capacity and the thermal conductivity in the gas phase depends on the temperature and the concentration, and are calculated as described in (19-20).

Ohmic polarization occurs due to resistance of the flow of ions in the electrolyte and electrical resistance in the electrodes. The electrodes and electrolyte are heated due to this effect, and calculated as described in (19-20). The inlet gas temperature is defined by the operating conditions and the outlet one is defined as a convective flux. The boundaries at the top and bottom of the cell are defined by symmetry, because it is assumed that the cell is surrounded by other cells with the same temperature distribution. The heat flux between the electrodes/interconnect and gas channels are specified at two channel walls, located opposite to each other, with a constant Nusselt number (4.094) from (24), based on the fully developed flow for a rectangular duct (aspect ratio is 1 for both channels). The cell is also heated due to change in entropy in the electrochemical reactions, concentration- and activation polarizations. These effects are defined at the electrolyte/electrode interfaces, where the electrochemical reactions are defined (19-20).

Internal reforming reactions

Nickel/zirconia is usually used as the material in SOFC anodes, and sufficient activity for the steam reforming reaction is provided (25). Reaction kinetics from (26) for the steam reforming (an expression dependent on surface area ratio) and the water-gas shift reactions are used to calculate the reaction velocity in this work. Other global kinetic

models can be found in (27,28). The catalytic steam reforming reaction occurs at the surface of the nickel catalyst and is specified as (26):

$$r_r = SA \cdot \left(63.6 \cdot T^2 \cdot \exp\left(\frac{-27063}{T}\right) \cdot c_{CH_4} c_{H_2O} - 3.7 \cdot 10^{-14} \cdot T^4 \cdot \exp\left(\frac{-232.78}{T}\right) \cdot c_{CO} c_{H_2}^3 \right) \quad [12]$$

where c is the gas species concentration, T the temperature, r the reaction rate and SA the surface area ratio. Different approaches for defining the water-gas shift reaction can be found in literature: **1.** Global reaction mechanism that considers reaction in the anode (10,13). **2.** Global reaction mechanism that considers reaction in the anode and in the fuel channel (6,26). **3.** A more advanced reaction mechanism that includes catalytic surface reaction kinetics for steam reforming, water-gas shift reaction and the Boudouard mechanism can be found in (9,29). It is frequently stated in literature (6,26,28) that the water-gas shift reaction should be considered to be in (or very close to) equilibrium state. The approach in (26) that considers reaction in the anode and in the fuel channel has been selected for this study:

$$r_s = 1199 \cdot T^2 \cdot \exp\left(\frac{-12509}{T}\right) \cdot c_{CO} c_{H_2O} - 6.77 \cdot 10^4 \cdot T^2 \cdot \exp\left(\frac{-16909}{T}\right) \cdot c_{CO_2} c_{H_2} \quad [13]$$

The source terms (to be implemented in the Maxwell Stefan equation for mass transport), due to the catalytical reforming reactions, are defined as (13):

$$S_{H_2} = \left(3r_r + r_s\right) \cdot M_{H_2} \quad [14]$$

$$S_{CH_4} = -r_r \cdot M_{CH_4} \quad [15]$$

$$S_{H_2O} = \left(-r_r - r_s\right) \cdot M_{H_2O} \quad [16]$$

$$S_{CO} = \left(r_r - r_s\right) \cdot M_{CO} \quad [17]$$

where M_i is the molecular weight of spices i, and S_i the source term of species i. The last species (CO_2) can be solved because the sum of the mass fractions equals unity. The heat generation/consumption due to the reforming reaction is specified in eq. [18] and the enthalpy change due to reaction is taken from (19).

$$Q_{\text{int}.ref} = \sum_i r_i \cdot \Delta h_{reaction,i} \quad [18]$$

where Δh_r is the enthalpy change due to the reactions and Q is the heat generation.

Results and Discussion

The fuel gas inlet conditions are specified as $x_{H2} : x_{CH4} : x_{CO} : x_{H2O} : x_{CO2} = 0.2626 : 0.171 : 0.0294 : 0.4934 : 0.0436$ (defined by IEA) (27), and the gas inlet temperature is specified as 1100 K. An average cell current density of 0.3 A/cm^2, an oxygen surplus factor of 4, fuel consumption of 80 % (mole) and flow direction left -> right for both the

anode and the fuel channel, are defined. Typical SOFC material characteristic data used in this work are found in (19-20). An anode surface area ratio of 619000 m²/m³ (23) is used for the basic case (named **a**), and increased with a factor 10 (named **b**) to study the effect of surface area ratio on steam reforming reaction rate and on the related mole fraction distributions.

The steam reforming reaction (eq. [4]) proceeds in the anode at the Ni-catalyst surfaces and the reaction rate can be seen in Fig. 2. An increased surface area ratio (**b**) means an increased reaction rate close to the fuel channel inlet where the concentration of methane is high and obvious a faster conversion of methane to carbon monoxide and hydrogen.

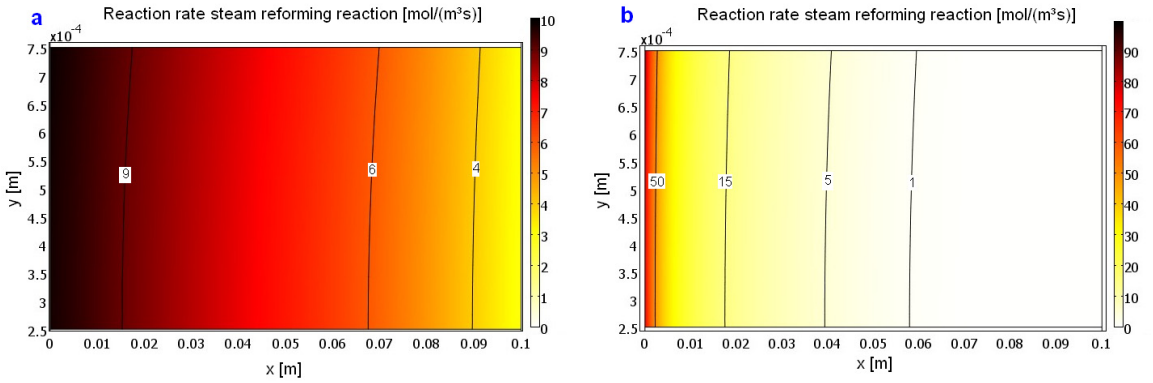

Figure 2. Surface area ratio effects on steam reforming reaction rate in the anode.

The reaction rate for the water-gas shift reaction as shown in Fig. 3, is highest in the anode close to the fuel channel inlet where the production of carbon monoxide is high, due to the steam reforming reaction. The water-gas shift reaction proceeds in the anode as well as in the fuel channel. The reaction rate is higher in the anode compared to the fuel channel, because the steam reforming as well as the electrochemical reactions occurs within the anode. As hydrogen is consumed and steam generated due to the electrochemical reactions the water-gas shift reaction proceeds to the right and more hydrogen is generated. An increased surface area ratio (**b**) results in a quicker production of carbon monoxide and obviously a higher water-gas shift reaction rate close to the fuel inlet.

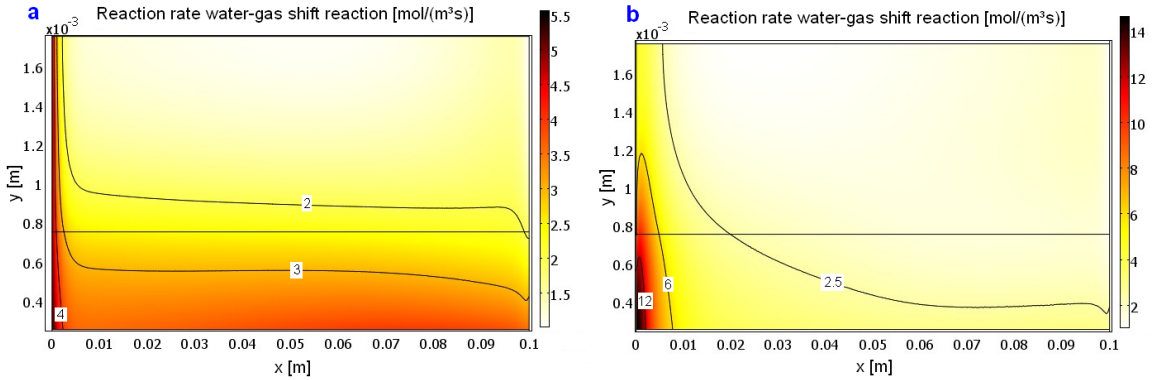

Figure 3. Surface area ratio effects on water-gas shift reaction rate in the anode and fuel channel.

The mole fraction distribution of methane can be seen in Fig. 4. The fraction difference in the y-direction is due to the catalytic steam reforming reaction (eq. [4]) in the porous structure. Methane diffuses from the channel towards the porous anode. Note that the fuel channel length is 100 times bigger than the channel height. An increased surface area ratio (**b**) means that the methane is faster converted into hydrogen and carbon monoxide.

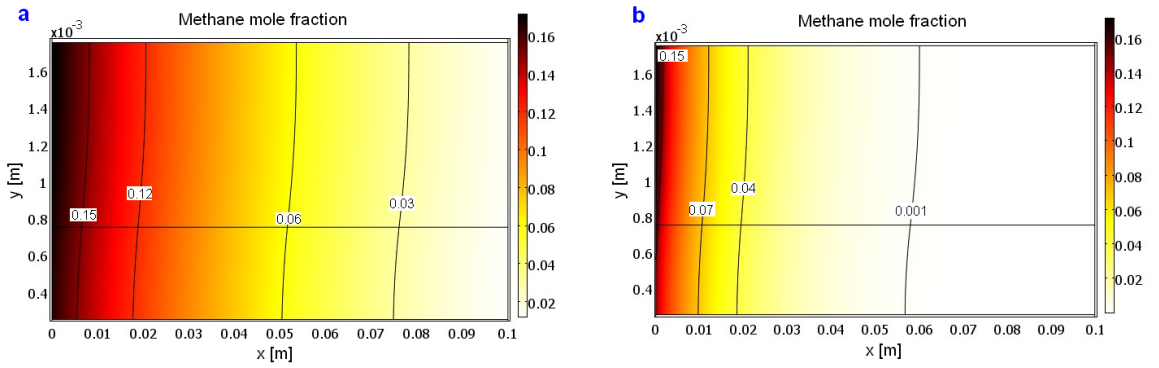

Figure 4. Surface area ratio effects on methane mole fraction.

The mole fraction distribution of carbon monoxide can be seen in Fig. 5. Carbon monoxide is generated within the porous anode structure as the methane is reformed, and then gradually converted to hydrogen and carbon dioxide (in the anode as well as in the fuel channel), due to the water-gas shift reaction. The fraction difference in the y-direction close to the inlet is because the methane reforming (eq. [4]) takes place in the anode (and not in the fuel channel). Carbon monoxide can participate in the electrochemical reactions (eq. [3]), but in this study it is neglected. An increased surface area ratio (**b**) means that the maximum carbon monoxide fraction become higher. This is due to the fact that the fraction of hydrogen is higher and the mole fraction of water lower, and the effect on the water-gas shift equilibrium reaction proceeds then to the left, i.e., getting a higher fraction of carbon monoxide.

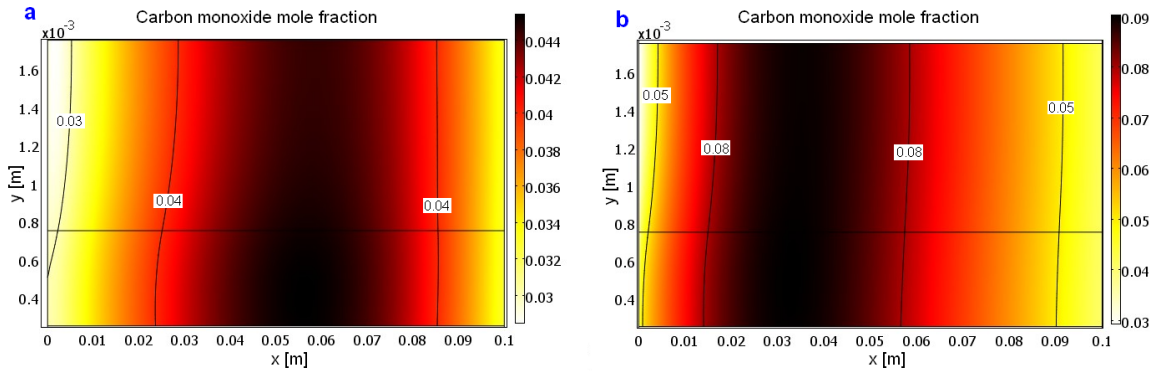

Figure 5. Surface area ratio effects on carbon monoxide mole fraction.

The mole fraction distribution of water can be seen in Fig. 6. Water is generated in the electrochemical reaction (eq. [2]) at the anodic TBP and consumed in the steam

reforming reaction (eq. [4]) and in the water-gas shift reaction (eq. [5]). The highest concentration is found at the outlet. For the case with an increased surface area ratio (**b**) the water decrease close to the inlet, because the steam reforming and the water-gas shift reaction consume more water, than the electrochemical reaction generates.

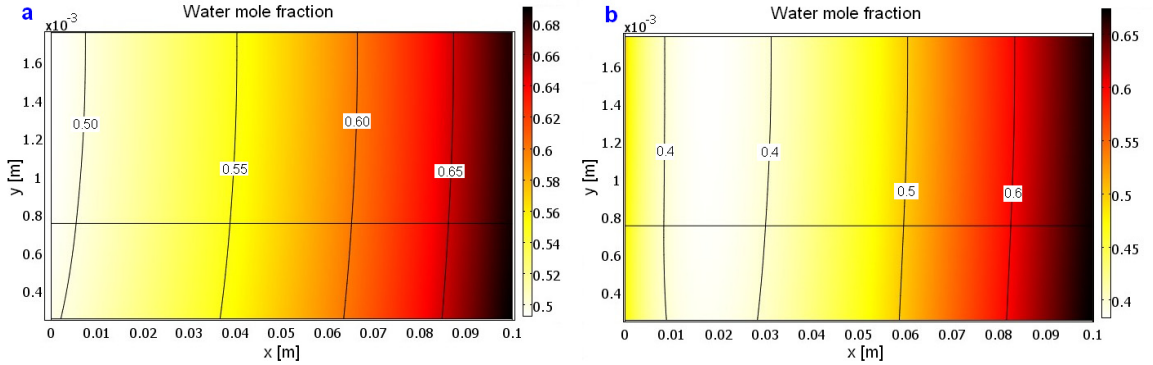

Figure 6. Surface area ratio effects on mole fraction of water.

Hydrogen is consumed at the anodic TPB, where the electrochemical reaction takes place (eq. [2]). In the case with the bigger surface area ratio (**b**) the highest hydrogen fraction along the flow direction can be found where most of the methane is converted (Fig. 7). For the case with smaller surface area ratio (**a**) the fraction of hydrogen decreases along the flow direction. This difference is because the catalytic steam reforming and the water-gas shift reaction produces hydrogen faster, than hydrogen is consumed in the electrochemical reactions, for the case in (**b**).

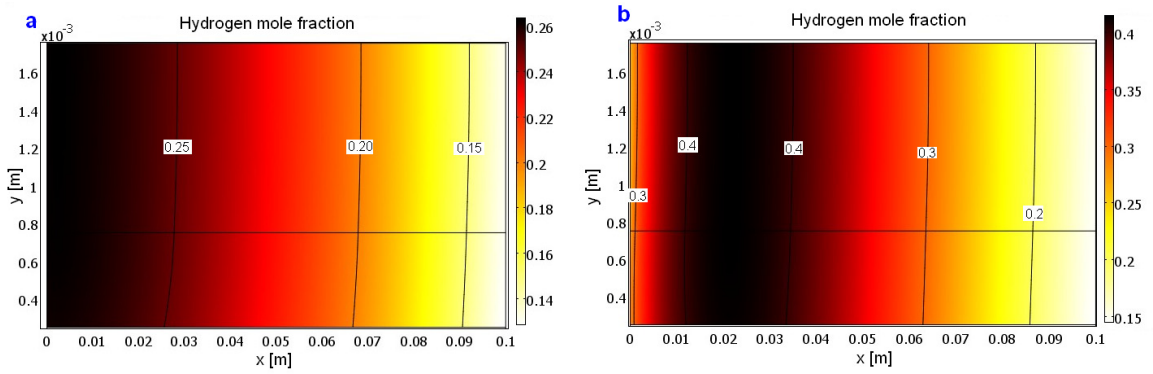

Figure 7. Surface area ratio effects on mole fraction of hydrogen.

Conclusion

In this study, a CFD approach is developed and implemented to analyze physical phenomena that take place inside an anode-supported SOFC. Equations for heat-, mass- and momentum transport are solved simultaneously. A LTNE approach is applied to calculate the temperatures in the solid phase and gas phase separately. The surface area ratio is varied to study the effect on reforming reaction rates and mole fraction distribution. An increased surface area ratio makes the conversion of methane to

hydrogen and carbon monoxide faster. Consumption of hydrogen and production of water at the anodic TPB along the flow direction make the water-gas shift reaction to proceed to the right (and produce more hydrogen).

Acknowledgments

The Swedish Research Council (VR) supports the current research.

References

1. Y. Patcharavorachot, A. Arpornwichanop and A. Chuachuebsuk, *J. Power Sources*, **177**, 254-261 (2008).
2. M. Andersson, J. Yuan and B. Sundén, Proceedings of *Heat Transfer 2008,* WIT Press, UK (2008)
3. M. Saxe, Doctoral thesis, KTH, Sweden (2008)
4. J. Yuan, G. Yang, M. Andersson and B. Sundén, Proceedings of *7th International Symposium on Heat Transfer (ISHT7),* Beijing, China (2008)
5. K. Reifsnider, X. Huang, G. Ju, R. Solasi, *J. Mater. Sci.*, **41**, 6751-6759 (2006)
6. P. Aguiar, C.S. Adjiman and N.P. Brandon, *J. Power Sources* **138**, 120-136 (2004)
7. H. Zhu, R. Kee, V. Janardhanan, O. Deutschmann and D. Goodwin, *J. Electrochem. Soc.*, **152**, A2427-A2440 (2005)
8. J.B. Gooenough and Y. Huang, *J. Power Sources*, **173**, 1-10 (2007)
9. V. Janardhanan and O. Deutschmann, *J. Power Sources*, **162**, 1192-1202, (2006)
10. M. Ni, M.K.H. Leung and D.Y.C. Leung, *J. Power Sources*, **168**, 369-378 (2007)
11. M. Kemm, Doctoral thesis, Lund University, Sweden (2006)
12. M. Hussein, X. Li. and I. Dincer, *Int. J. Thermal Sciences*, **46**, 48-86 (2007)
13. J. Yuan, Y. Huang, B. Sundén and W.G. Wang, *Heat Mass Transfer*, **45**, 471-484 (2009)
14. R. Suwanwarangkul, E. Croiset, M.W. Fowler, P.L. Douglas, E. Entchev, M.A. Douglas, *J. Power Sources*, **122**, 9-18 (2003)
15. K. Tseronis, I.K. Kookos and C. Theodoropoulos, *Chem. Eng. Sci.*, **63**, 5626-5638 (2006)
16. M. Le Bars and M.G. Worster, *J. Fluid Mech.*, **550**, 149-173 (2006)
17. COMSOL Multiphysics 3.5 user guide, 2008
18. H.K. Versteeg and W. Malalasekera, An Introduction to Computational Fluid Dynamics, The Finite Volume Method, Pearson, UK (1995)
19. M. Andersson, Licentiate thesis, Lund University, Sweden (2009)
20. M. Andersson, J. Yuan, B. Sundén and W.G. Wang, Proceedings of 7th *International Fuel Cell Science, Engineering & Technology Conference*, Newport Beach, California, USA (2009)
21. D.L. Damm and A.G. Fedorov, *J. Power Sources*, **159**, 1153-1157 (2006)
22. C.H. Chao and A.J.J. Hwang, *J. Power Sources*, **160**, 1122-1130 (2006)
23. D. Marrero-López, J.C. Ruiz-Morales, J. Peña-Martínez, J. Canales-Vázquez and P. Núñez, *J. Solid State Chemistry*, **181**, 685-692 (2008)
24. R.K. Shah and A.L. London, Laminar Flow Forced Convection in Ducts. Academic Press, London, UK, 1978
25. J.R. Ferguson, J.M. Fiard, and R. Herbin, *J. Power Sources,* **58**, 109-122, (1996)
26. J.-M. Klein, Y. Bultel, S. Georges and M. Pons, *Chem. Eng. Sci.*, **62**, 1636-1649 (2007)
27. F. Nagel, T. Schildhauer, S. Biollaz and S. Stucki, *J. Power Sources*, **184**, 129-142 (2008)
28. D. Sanchez, R. Chacartegui, A. Munoz and T. Sanchez, *Int. J. Hydrogen Energy*, **33**, 1834-1844 (2008)
29. P.Hofmann, K.D. Panopoulos, L.E. Fryda, E. Kakaras, Energy, 1-7 (2008)